DOI: https://doi.org/10.54966/jreen.v26i2.1145 - *Journal of Renewable Energies 26 (2023) 179 – 188*

Journal of Renewable Energies

Revue des Energies Renouvelables

journal home page : https://revue.cder.dz/index.php/rer

Research paper

CFD study of active flow control around a wind turbine profile using synthetic jet

Ali Boudis [a,*], **Madjid Tata** [a] , **Ahmed Bekhti** [a] , **Dawoud Hamane** [a]

[a] *Centre de Développement des Energies Renouvelables, CDER, BP 62 Route de l'Observatoire, Bouzaréah, 16340, Algiers, Algeria*

ARTICLE INFO

Article history:
Received August 7, 2023
Accepted September 26, 2023

Keywords:
Flow control,
Synthetic jet,
S809 airfoil,
Wind turbine,
CFD.

ABSTRACT

In this study, numerical simulations are performed to investigate the effect of the position and jet angle of the synthetic jet on the aerodynamic characteristics of a wind turbine blade profile. The study is applied to the NREL S809 profile with a 1m chord, set at an angle of attack of 15.2° in a flow at a Reynolds number $Re = 10^6$. The synthetic jet is placed on the extrados of the profile and modeled by a sinusoidal function. The flow around the blade profile is simulated by solving Navier–Stokes equations using the commercial software ANSYS Fluent based on the finite volume method. Turbulence is simulated using the two-equation $SST - k\omega$ model. The results show that the considered jet parameters have a strong effect on the aerodynamic characteristics of the profile. Applying an optimal combination of synthetic jet parameters significantly improves the aerodynamic performance of the profile.

1. INTRODUCTION

In recent years, the depletion of fossil fuel supplies, along with environmental concerns about greenhouse gas emissions, is spurring research into clean and renewable energy sources. Wind energy is one of the most promising and sustainable sources. This type of energy is obtained by converting the kinetic energy of the wind into mechanical energy that can be used to generate electricity or pump water. Blades are the primary element on which wind acts. They are frequently affected by the undesirable phenomenon of boundary layer separation, which causes several problems such as increased drag and decreased lift, blade vibrations, and noise generation due to strong vortices in the detached zones. As a

* *Corresponding author, E-mail address: a.boudis@cder.dz*
Tel : + 213 540080992

ISSN: 1112-2242 / EISSN: 2716-8247

solution to this problem, several flow control techniques were used in the design of wind turbine blade (Akhter & Omar, 2021; Manerikar et al., 2021). One of these techniques is the synthetic jet actuator, which is a device that oscillates a diaphragm placed on one (or more) walls of a sealed cavity to generate a synthesized jet from the ambient fluid through an orifice or slot (Gul et al., 2014).

In a recent review by Chiatto and De Luca (2023), it is shown that synthetic jets were extensively used for flow control on aerodynamic surfaces or to improve cooling of heated areas. As far as we are concerned, we are interested in the control of the flow around the profile of wind turbines. For this purpose, Mallinson et. Al. (2023) investigated a synthetic flow control using both experimental and computational methods. This study first concerned the flow generated by circular orifices, then applications to the flow control over a circular cylinder and to the enhancement of the mixing in a flame were considered. Later on, a Plasma Synthetic Jet (PSJ) actuator was developed at ONERA where the PIV technique was used to assess the device's efficiency. The actuation-induced decrease in separated flow region and consequently drag reduction of a NACA 0015 airfoil was estimated (Caruana et al., 2013). Montazer et al. (2016) performed numerical computations for flow control around NACA 0015 profile using synthetic jet. They showed that the synthetic jet parameters must be optimized for improving aerodynamic performance. Zong et al. (2018) provides a review of the development of PSJ technology and its application to flow control at moderate to high-Reynolds number. More recently, Botero et al. (2022) present the results of simulations on a straight-bladed Darrieus turbine using synthetic jets as a flow control method. Wang et al. (2022) applied a dual synthesis jets actuator to the trailing edge of VAWT. They performed numerical and experimental investigations and proposed an arrangement that can effectively improve the power capacity of VAWT.

This brief review shows that the use of synthetic jets for flow control is still relevant and that various parameters influence the performance of this type of control. For this purpose, numerical simulations were carried out to investigate the effects of the jet parameters on flow control around an NREL S809 wind turbine airfoil. In a previous study (Boudis et al., 2015), the influence of jet frequency and amplitude was studied. In this paper, the effect of synthetic jet location and inclination on the aerodynamic performance and flow structure around the airfoil is considered. This study is applied to the S809 profile with a 1m chord, set at an angle of attack of 15.2° in a flow at a Reynolds number $Re = 10^6$.

2. NUMERICAL APPROACH

The flow around the blade profile is simulated by solving the Reynolds averaged Navier–Stokes equations. The synthetic jet is defined as a velocity inlet boundary condition through a small orifice located on the extrados of the profile.

2.1 Synthetic jet model

The synthetic jet is modeled using a sinusoidal function as follows:

$$U_j(t) = U_{j,max}\ \sin(2\pi f_j t) \tag{1}$$

Where $\boldsymbol{U_{max,j}}$ is the maximal jet velocity, $\boldsymbol{f_j}$ is the jet frequency**.**

The efficiency of the synthetic jet control is influenced by several parameters such as the maximal jet velocity ($\boldsymbol{U_{max,j}}$), jet position ($\boldsymbol{X_j}$), jet width ($\boldsymbol{D_j}$), and jet angle ($\boldsymbol{\theta_j}$) (see Fig. 1).

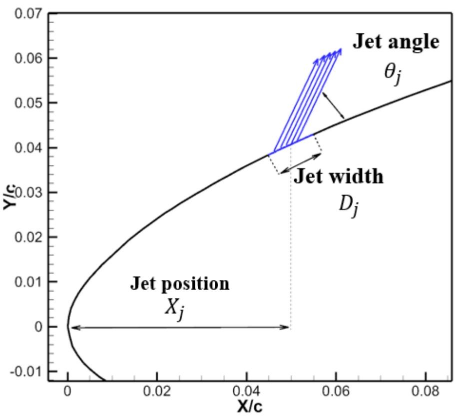

Fig. 1. Synthetic jet configuration.

The three dimensionless parameters commonly used to investigate active flow control by synthetic jet are given below:

- Non-dimensional jet amplitude

$$\boldsymbol{a_j} = \frac{\boldsymbol{U_{j,max}}}{\boldsymbol{U_\infty}} \tag{2}$$

- Non-dimensional jet frequency

$$\boldsymbol{F^*} = \frac{\boldsymbol{f_j\, c}}{\boldsymbol{U_\infty}} \tag{3}$$

- Momentum Coefficient

$$C_\mu = \frac{\rho_j D_j U_{j,max}^2}{0.5\, \rho_\infty\, c\, U_\infty^2} \tag{4}$$

where U_∞ is the flow velocity, ρ_∞ is the free-stream fluid density, and ρ_j is the jet flow fluid density and c is the airfoil chord.

2.2 Fluid Equations

The governing equations are solved in a 2D computational domain. The unsteady and incompressible Reynolds averaged Navier–Stokes equations write as follows:

$$\frac{\partial u_x}{\partial x} + \frac{\partial u_y}{\partial y} = 0 \tag{5}$$

$$\frac{\partial u_x}{\partial t} = -u_x \frac{\partial u_x}{\partial x} - u_y \frac{\partial u_x}{\partial y} - \frac{1}{\rho}\frac{\partial p}{\partial x} + (\nu + \upsilon_T)\left(\frac{\partial^2 u_x}{\partial x^2} + \frac{\partial^2 u_x}{\partial y^2}\right) \tag{6}$$

$$\frac{\partial u_y}{\partial t} = -u_x \frac{\partial u_y}{\partial x} - u_y \frac{\partial u_y}{\partial y} - \frac{1}{\rho}\frac{\partial p}{\partial y} + (\upsilon + \nu_T)\left(\frac{\partial^2 u_y}{\partial x^2} + \frac{\partial^2 u_y}{\partial y^2}\right) \tag{7}$$

where t is the time, u_x and u_y are velocity component, p is the pressure, ν and $\nu_t$are the laminar and turbulent kinematic viscosity, respectively.

In this study, the turbulence is simulated by the two-equation $SST\ k-\omega$ model (Menter, 1994). This model is a combination of the $k-\varepsilon$ and $k-\omega$ models. It uses the $k-\omega$ model near the wall and switches to a $k - \varepsilon$ model away from the wall. The turbulent kinetic energy k and the specific dissipation rate ε in the SST k-ω model write as:

$$\frac{\partial k}{\partial t} + u_j \frac{\partial k}{\partial x_j} = P_k - \beta^* k\omega + \frac{\partial}{\partial x_j}\left[(\upsilon + \sigma_k \upsilon_T)\frac{\partial k}{\partial x_j}\right] \tag{8}$$

$$\frac{\partial \omega}{\partial t} + u_j \frac{\partial \omega}{\partial x_j} = \beta S^2 - \alpha\omega^2 + \frac{\partial}{\partial x_j}\left[(\upsilon + \sigma_\omega \upsilon_T)\frac{\partial \omega}{\partial x_j}\right] + 2(1 - F_1)\sigma_{\omega 2}\frac{1}{\omega}\frac{\partial k}{\partial x_i}\frac{\partial \omega}{\partial x_i} \tag{10}$$

Further details on model parameter definitions are available in the reference (Menter, 1992). The SST k-ω turbulence model has been successfully applied in many wind turbine flow simulations, including the works of Karbasian et al. (2016), Vučina et al.(2016), Boudis et al. (2018), Boudis et al. (2023), and many others.

2.3 Flow solver

The unsteady flow field around the S809 profile was simulated using the finite volume code ANSYS Fluent. A segregated pressure-based solver was used to solve the Navier–Stokes equations with a pressure–velocity coupling achieved by the coupled algorithm. For the spatial gradient discretization, a Green-Gauss Cell-based approach is applied. The pressure and momentum terms are discretized using the second-ordered scheme and the second-order Upwind method, respectively. The first-order Upwind method is used to calculate the turbulent kinetic energy and dissipation rate. For all simulations, maximal numbers of iterations per time step and target residuals for convergence are set to 70 and 10^6, respectively.

2.4 Computational grid and boundary conditions

The size of the computational domain and the boundary conditions used are illustrated in Fig. 2. The study area extends over 60D in width and 30D in height. The origin of the coordinates is located 15D from the left, bottom, and top boundaries, and 45D from the right boundary. The computational domain is divided into two areas, an inner circular part, surrounded by a rectangular part. The circular zone contains the profile so it is meshed with a fine quadrilateral mesh to capture the physical gradients close to the wall. The height of the row of cells around the airfoil is $4\ 10^{-5}$c so that the dimensionless y^+ is lower than 1. Far from the profile, in the rectangular zone, the mesh is less dense to limit the total number of cells and the calculation time. The connection between the two zones is made using non-formal interfaces.

Boundary conditions. At the inlet, up, and bottom boundaries, the velocity-inlet condition is defined with the pressure set to zero gradient and the x-component of the fluid velocity defined according to the specified Reynolds number. At the outlet boundary, the pressure outlet is set with the pressure equal to the free flow pressure, and the outlet velocity is set to zero. On the profile surface, the no-slip condition is imposed with a periodic velocity inlet condition at the synthetic jet location.

2.5 Grid and Time Step Independence Study

A sensitivity analysis is performed to check the independence of the numerical solution on the grid and the time step. First, the dependence of the spatial resolution on the results was investigated. Thus, four Mesh of different densities are considered: Mesh-1 built of 31100 cells (with 200 points over the profile surface), Grid-2 constructed with 61850 cells (with 400 points over the profile surface), Grid-3 composed of 84850 cells (with 600 points over the profile surface), and Grid-4 which consists of 126300 cells (with 800 points over the profile surface). The mesh independence study is conducted for the uncontrolled profile at $Re = 10^6$and $AoA = 15.2°$ using the time step $\Delta t =\ 10^{-4}$ s. The lift and drag coefficients obtained are summarized in Table 1. It can be seen that the difference between the results obtained with Mesh-3 and Mesh-4 is negligible. Therefore, Mesh-3 is considered fine enough to produce reliable results and is applied to the calculations that follow.

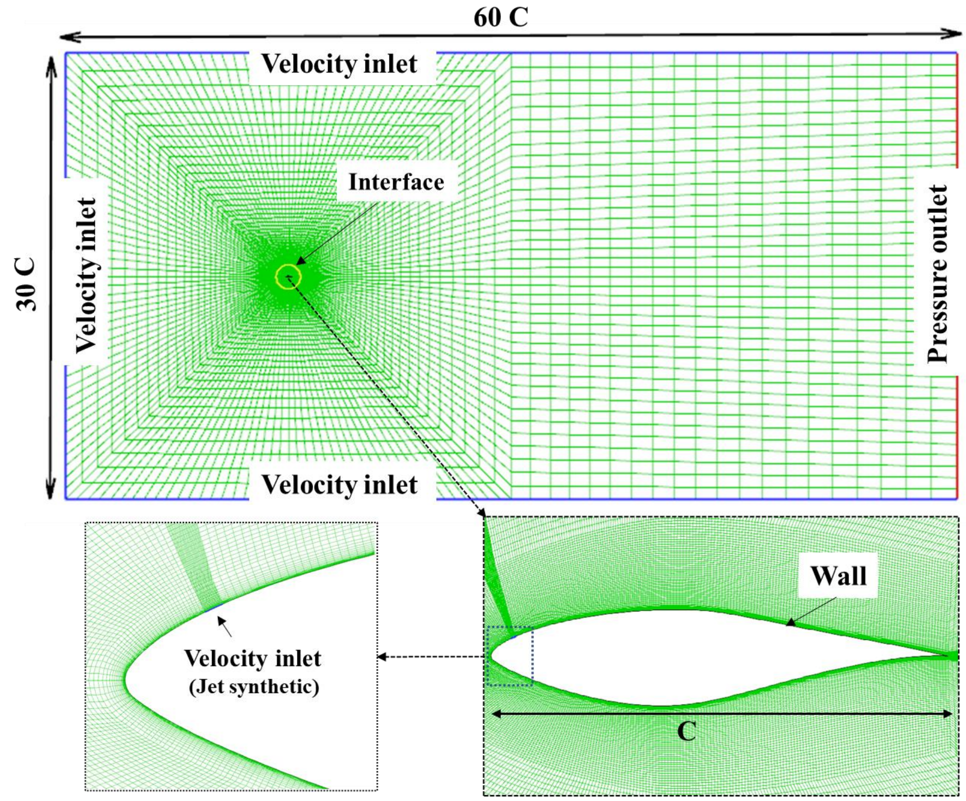

Fig. 2. Computational domain and boundary conditions.

Then, the study of independence of the time step on the numerical results is carried out using three different time steps: $T/20$, $T/50$, and $T/100$ where T is the period ($T = 1/f$). This study is conducted for the controlled profile using the following synthetic jet parameters: $X_j = 30\%c, D_j = 1\%c , \theta_j = 20°, a_j = 3$, and $F^* = 4$. As can be seen in Table 2, the results obtained with T/50 are close to those obtained with T/100. The difference between the lift-to-drag ratio is 1.2%. Therefore, the time-step $\Delta t = T/50$ is applied to all subsequent simulations.

Table.1 Mesh independence study

Mesh	Mesh on airfoil	Total cell	C_L	C_D	C_L/C_D
Mesh-1	200	31100	1.0216	0.0801	12.7541
Mesh-2	400	61850	1.159	0.0644	17.9969
Mesh-3	600	84850	1.1921	0.064	18.6266
Mesh-4	800	126300	1.1977	0.0639	18.7435

Table.2 Time step independence study

Time-step	C_L	C_D	C_L/C_D
T/20	1.7711	0.0255	69.4544
T/50	1.7615	0.0261	67.4904
T/100	1.7533	0.0263	66.6654

2.5 Model validation

To assess the accuracy of the applied solver, numerical simulations were performed for an S809 airfoil without flow control, set at different angles of attack in the range (0°-20°). The obtained results are compared to experimental data (Ramsey et al., 1995; Somers, 1997) and published numerical results (Johansen, 1999; Zhong et al., 2017). Fig. 3 shows that the computed lift and drag coefficients are in good agreement with the experimental data up to an angle of attack of about 9°. At larger angles (> 9°), the difference with experimental data is visible. Nevertheless, at all angles of attacks, the current computational results are in good agreement with published computational results.

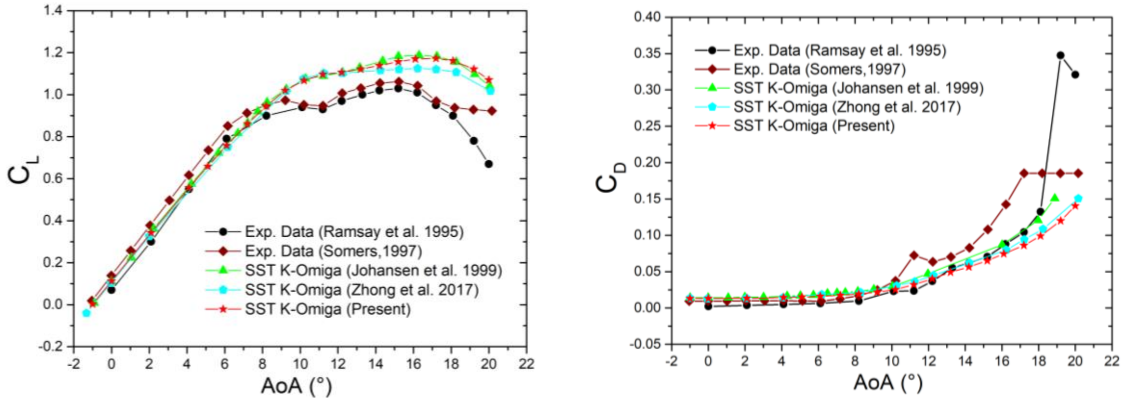

(a) (b)

Fig. 3. Lift (a) and drag (b) coefficients as a function of the angle of attack at $Re = 10^6$.

3. RESULTS AND DISCUSSION

The effects of synthetic jet location (X_j) and jet angle (θ_j) on the aerodynamic performance and flow structure around the wind turbine blade profile are carried out by applying the other synthetic jet parameters set as follows: $D_j = 1\%c$, $a_j = 3$, and $F^* = 4$. The results obtained with control are compared with the results without control to show the influence of these parameters on the aerodynamic characteristics of the profile.

3.1 Influence of synthetic jet location

These simulations are performed for an inclination of the jet $\boldsymbol{\theta_j = 15°}$. Fig. 4 shows the lift-to-drag ratio variations of the controlled airfoil for different jet synthetic locations, varying from 5%c to 90%c. This figure shows that the best improvement in the airfoil lift-to-drag ratio is obtained when the synthetic jet is located in the area (30%c-50%c) from the leading edge. This is due to the flow separation that occurs just near the position of 50%c on the upper surface of the airfoil. Placing the synthetic jet after the separation point decreases the efficiency of the synthetic jet. These results show that the best location for the synthetic jet is just before the separation point.

Fig. 5 presents the pressure coefficient and pressure contours around the S809 profile for both cases, without and with control, for a jet located at ($\boldsymbol{X_j = 30\%c}$). (From this figure it can be seen that the synthetic jet has a large influence on the pressure distribution around the profile. Under the effect of a synthetic jet, the pressure difference between the upper and lower surface is increased, which leads to improving lift.

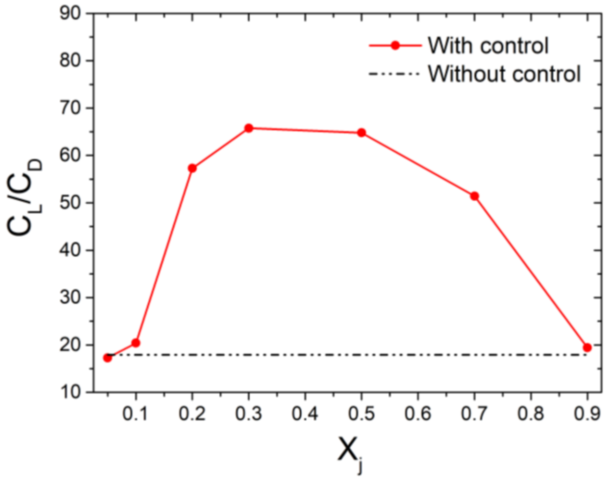

Fig. 4. Variation of the lift-to-drag ratio with the jet position

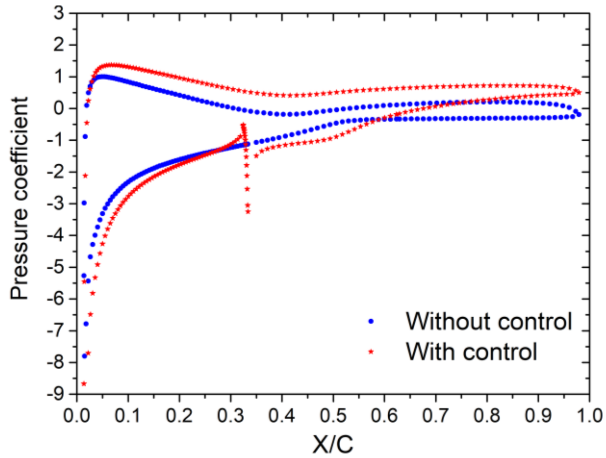

(a)

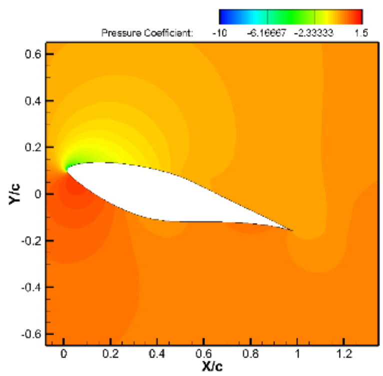

(b)

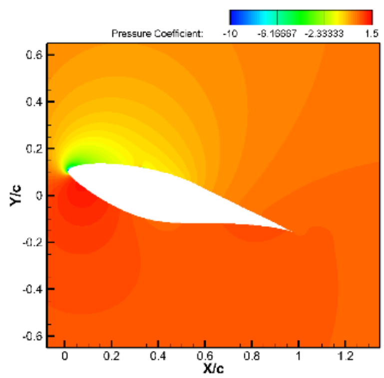

(c)

Fig. 5. Pressure coefficient (a) and contours of pressure around the reference (b) and controlled (c) profiles, ($\boldsymbol{X_j = 30\%c}$).

3.2 Influence of synthetic jet inclination

The influence of jet angle is investigated for a synthetic jet actuator placed at 30%c from the leading edge. The jet angle is varied from 5° to 45°. Fig. 6 shows the variation of the lift-to-drag ratio as a function of the synthetic jet angle. The results obtained show that all synthetic jet angles investigated in this study improve the aerodynamic performance of the S809 airfoil compared to the case without control. The control efficiency rises with increasing jet angle up to a threshold angle, $\theta_j = 20°$, beyond this angle, increasing the jet angle reduces control efficiency.

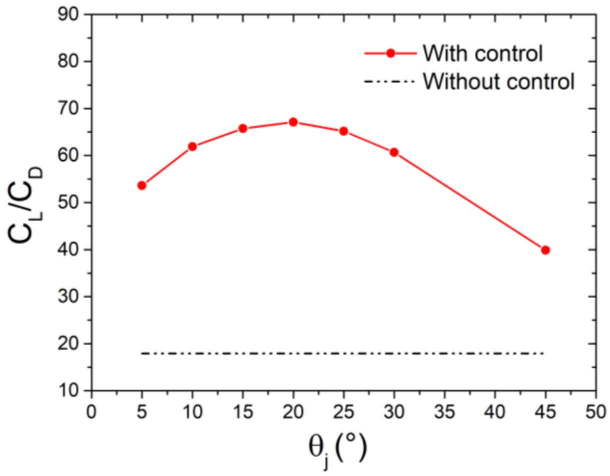

Fig. 6. Variation of lift-to-drag ratio with the jet inclination.

3.3 Flow structure around the airfoil

The streamlines and the x-velocity fields around the airfoil, without and with flow control, are shown in Fig.7, with the synthetic jet parameters set to: $\boldsymbol{D_j = 1\%c}$, $\boldsymbol{a_j = 3}$, $\boldsymbol{F^* = 4, \theta_j = 15°\ and\ X_j = 0.3c}$. This figure shows that under the effect of the synthetic jet, the separation point moves towards the trailing edge and the size of the recirculation zone decreases.

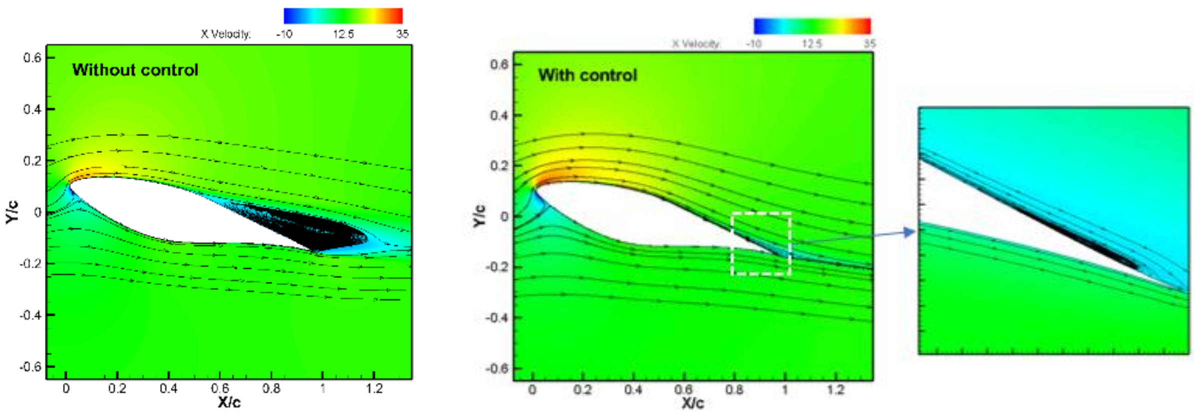

(a) (b)

Fig. 7. Streamline and contours of the x-velocity component around the airfoil without (a) and with control (b).

4. CONCLUSION

In this study, the effects of synthetic jet location and inclination on the aerodynamic performance and flow structure around a wind turbine blade profile are investigated. The control was applied to an S809 airfoil at $\boldsymbol{Re = 10^6}$, set at an angle of attack of $\mathbf{15.2}°$, and a synthetic jet actuator located on the upper surface of the airfoil. The main results of this study are summarized as follows:

- The synthetic jet has a significant effect on the aerodynamic characteristic and flow structure around the airfoil.
- The best location for the synthetic jet is just before the separation point.
- The use of an optimized synthetic jet angle significantly improves the lift-to-drag ratio of the airfoil.
- The recirculation zone on the upper surface of the profile is greatly reduced under the effect of synthetic jet control.

In future works, further investigations are planned to study the influence of the airfoil shape by considering other wind turbine airfoils. The evaluation of the power performance improvement of a wind turbine built with a flow-controlled blade will also be considered.

NOMENCLATURE

AoA	Angle of attack [°]	t	Time [s]
a_j	Non-dimensional jet amplitude	T	Period
c	Airfoil chord [m]	$U_{j,max}$	Maximal jet velocity [m/s]
C_D	Drag coefficient	U_∞	Flow velocity [m/s]
C_L	Lift coefficient	X_j	Jet position [m]
C_μ	Momentum coefficient	ρ_∞	Free-stream fluid density [kg/m^3]
D_j	Jet width [m]	ρ_j	Jet flow fluid density [kg/m^3]
f_j	Jet frequency [Hz]	θ_j	Jet angle [°]
F^*	Non-dimensional jet frequency		

REFERENCES

Akhter, M. Z. and Omar, F.K. Review of Flow-Control Devices for Wind-Turbine Performance Enhancement, Energies 2021, Vol. 14, Page 1268, vol. 14, no. 5, p. 1268, Feb. 2021, doi: 10.3390/EN14051268.

Botero, N., Ratkovich, N., Lain, S. and Lopez Mejia, O.D. Synthetic jets as a flow control device for performance enhancement of vertical axis hydrokinetic turbines: A 3D computational study, Heliyon, vol. 8, no. 8, p. e10017, Aug. 2022, doi: 10.1016/J.HELIYON.2022.E10017.

Boudis, A., Guerri, O., Benzaoui, A. and Oualli, H. Contribution à l'étude du contrôle actif de l'écoulement autour d'un profil de pale d'éolienne, Revue des Energies Renouvelables, vol. 18, no. 3, pp. 417–428, Sep. 2015, Accessed: Aug. 07, 2023. [Online]. Available: https://www.asjp.cerist.dz/en/article/121282.

Boudis, A., Guerri, O., Oualli, H. and Benzaoui, A. Aerodynamic optimization of active flow control over S809 airfoil using synthetic jet, 2018 Int. Conf. Wind Energy Appl. Alger. ICWEAA 2018, Jan. 2019, doi: 10.1109/ICWEAA.2018.8605084.

Boudis, A., Hamane, D., Guerri, O. and Bayeul-Lainé, A.C. Airfoil Shape Optimization of a Horizontal Axis Wind Turbine Blade using a Discrete Adjoint Solver, J. Appl. Fluid Mech., vol. 16, no. 4, pp. 724–738, 2023, doi: 10.47176/jafm.16.04.1493.

Caruana, D., Rogier, F., Dufour, G. and Gleyzes, C. The Plasma Synthetic Jet Actuator, Physics, Modeling and Flow Control Application on Separation, Aerosp. Lab, no. 6, pp. 1–13, 2013, [Online]. Available: https://hal.science/hal-01184643.

Chiatto, M. and De Luca, L. Advances in Flow Control by Means of Synthetic Jet Actuators, Actuators 2023, vol. 12, p. 33, 2023, doi: 10.3390/act12010033.

Gul, M., Uzol, O. and Akmandor, I.S. An Experimental Study on Active Flow Control Using Synthetic Jet Actuators over S809 Airfoil, J. Phys. Conf. Ser., vol. 524, no. 1, p. 012101, Jun. 2014, doi: 10.1088/1742-6596/524/1/012101.

Johansen, J. Unsteady Airfoil Flows with Application to Aeroelastic Stability, Technical University of Denmark. Risø Reports No. R-1116, 1999.

Karbasian, H. R., Esfahani, J.A., and Barati, E. Effect of acceleration on dynamic stall of airfoil in unsteady operating conditions, Wind Energy, vol. 19, no. 1, pp. 17–33, Jan. 2016, doi: 10.1002/we.1818.

Mallinson, S., Australia, M., Reizes, J. and Hong, G. Synthetic jet actuators for flow control, 1999, Accessed: Aug. 07, 2023. [Online]. Available: https://www.researchgate.net/publication/253795787.

Manerikar, S. S. et al., Horizontal axis wind turbines passive flow control methods: a review, MS&E, vol. 1136, no. 1, p. 012022, Jun. 2021, doi: 10.1088/1757-899X/1136/1/012022.

Menter, F. R. Two-equation eddy-viscosity turbulence models for engineering applications, AIAA J., vol. 32, no. 8, pp. 1598–1605, 1994, doi: 10.2514/3.12149.

Montazer Wahhab Al-Jibory et al., Optimization of a synthetic jet actuator for flow control around an airfoil, IOP Conf. Ser. Mater. Sci. Eng., vol. 152, no. 1, p. 012023, Oct. 2016, doi: 10.1088/1757-899X/152/1/012023.

Ramsay, R., Hoffman, M. and Gregorek, G. Effects of Grit Roughness and Pitch Oscillations on the S809 Aerofoil, 1995.

Somers, D. M. Design and experimental results for the S809 airfoil, Jan. 1997, doi: 10.2172/437668.

Vučina, D., Marinić-Kragić, I., and Milas, Z., Numerical models for robust shape optimization of wind turbine blades, Renew. Energy, vol. 87, pp. 849–862, Mar. 2016, doi: 10.1016/j.renene.2015.10.040.

Wang, P. et al., Effect of trailing edge dual synthesis jets actuator on aerodynamic characteristics of a straight-bladed vertical axis wind turbine, Energy, vol. 238, p. 121792, Jan. 2022, doi: 10.1016/J.ENERGY.2021.121792.

Zhong, J., Li, J. and Guo, P. Effects of leading-edge rod on dynamic stall performance of a wind turbine airfoil, Proc. Inst. Mech. Eng. Part A J. Power Energy, vol. 231, no. 8, pp. 753–769, Dec. 2017, doi: 10.1177/0957650917718453.

Zong, H., Chiatto, M., Kotsonis, M. and de Luca, L. Plasma Synthetic Jet Actuators for Active Flow Control, Actuators 2018, Vol. 7, Page 77, doi: 10.3390/ACT7040077.